Dependence of Climate Response on Meridional Structure of External Thermal Forcing

SARAH M. KANG

School of Urban and Environmental Engineering, Ulsan National Institute of Science and Technology, Ulsan, South Korea

SHANG-PING XIE

Scripps Institution of Oceanography, University of California, San Diego, La Jolla, California

ABSTRACT

This study shows that the magnitude of global surface warming greatly depends on the meridional distribution of surface thermal forcing. An atmospheric model coupled to an aquaplanet slab mixed layer ocean is perturbed by prescribing heating to the ocean mixed layer. The heating is distributed uniformly globally or confined to narrow tropical or polar bands, and the amplitude is adjusted to ensure that the global mean remains the same for all cases. Since the tropical temperature is close to a moist adiabat, the prescribed heating leads to a maximized warming near the tropopause, whereas the polar warming is trapped near the surface because of strong atmospheric stability. Hence, the surface warming is more effectively damped by radiation in the tropics than in the polar region. As a result, the global surface temperature increase is weak (strong) when the given amount of heating is confined to the tropical (polar) band. The degree of this contrast is shown to depend on water vapor– and cloud–radiative feedbacks that alter the effective strength of prescribed thermal forcing.

1. Introduction

An important quantity in discussions of climate projections is how much the globe would warm in response to a unit increase of greenhouse gases. It is often implicitly assumed that the warming is proportional to the magnitude of global mean radiative forcing. It is a good approximation in many cases. Even the spatial distribution of climate change exhibits remarkable similarities when normalized to the same forcing for most climate forcing agents (Hansen et al. 2005; Xie et al. 2013). Although the radiative forcing for doubled CO_2 is well known to be in the range of 3.5–4.1 W m^{-2} (Ramaswamy et al. 2001), the envelop of large uncertainty in the prediction of global surface warming after a doubling of CO_2 concentration has not been narrowed appreciably for decades (Knutti and Hegerl 2008).

In fact, the global mean surface warming has been shown to be dependent on the climate forcing agents and their spatial distribution. Different climate forcing agents show a substantial range in the effectiveness for surface warming (Hansen et al. 2005). For example, the climate response to changes in CH_4 is larger than the climate response to a CO_2 forcing of the same magnitude at the top of the atmosphere (TOA). Also, the magnitude of surface warming depends on the meridional (Rose et al. 2014) and vertical structure of climate forcing (Hansen et al. 1997): extratropical radiative forcing yields a larger surface warming than tropical radiative forcing because of the sea ice feedback and the more stable lapse rate at high latitudes; a climate forcing that peaks at higher elevations tends to be less efficient in warming the surface since a larger fraction of the energy is radiated directly to space without warming the surface.

In general, the distribution of climate forcing agents such as aerosols, ice melt, and land use is highly localized. The present study investigates the dependence of global surface warming on the meridional distribution of climate forcing. We show that how the climate forcing is distributed meridionally matters significantly for the global surface warming. In particular, the global surface temperature response is weak when the thermal forcing is applied to the tropics compared with the case when

Corresponding author address: Sarah M. Kang, School of Urban and Environmental Engineering, Ulsan National Institute of Science and Technology, UNIST-gil 50, Ulsan 689-798, South Korea. E-mail: skang@unist.ac.kr

the thermal forcing is applied in the polar region, consistent with Hansen et al. (1997), Forster et al. (2000), and Joshi et al. (2003).

The most frequent types of perturbations used in the studies on radiative forcing and climate response are perturbations to the solar constant and carbon dioxide level. Here we consider perturbations to the surface energy budget in the model coupled to a slab mixed layer ocean. Our experiment setup is similar to perturbing the solar constant because its changes are mostly felt by the surface as little shortwave radiation is absorbed in the atmosphere. Changes in CO_2 are initially felt mostly by the midtroposphere, but it has been shown that the CO_2 and solar forcing experiments behave similarly (Forster et al. 2000; Joshi et al. 2003). Hansen et al. (2005) decompose climate change into fast and slow components defined as changes without and with ocean response. They define effective radiative forcing at TOA using an atmospheric GCM with fixed SST. By this definition, the global mean radiative imbalance at TOA equals net ocean surface flux. Thus, our results may be viewed as the slow response of Hansen et al. (2005) to radiative forcing.

2. Model and experiment setup

We employ two models of different level of complexity: the idealized moist GCM of Frierson et al. (Frierson et al. 2006; Frierson 2007) and an atmospheric general circulation model developed at the Geophysical Fluid Dynamics Laboratory (GFDL), Atmospheric Model, version 2 (AM2) (Anderson et al. 2004). The configuration of both models is the same as in Kang et al. (2008, 2009). We consider zonally symmetric aquaplanet simulations in which the atmosphere is coupled to 2.4-m-thick slab mixed layer ocean, corresponding to a heat capacity of $1 \times 10^7 \, \mathrm{J \, m^{-2} \, K^{-1}}$. A small heat capacity is chosen to reduce the time required for the model to reach equilibrium. The surface temperature is permitted to drop below freezing, and no sea ice or snow is allowed to form. Both models have no seasonal cycle of insolation but a diurnal cycle is retained in AM2. All simulations are spun up for two years, and statistics are calculated over six subsequent years of integration.

The key simplification in the idealized moist GCM is in the model physics that includes gray radiative transfer, in which the radiative fluxes are only a function of temperature, so that there are no water vapor– and cloud–radiative feedbacks. Hereafter, the idealized GCM will be referred to as GRaM. The shortwave heating approximates the observed annual and zonal mean TOA net shortwave flux. There is no solar absorption within the atmosphere and the surface albedo is set to be 31%. It is run at spectral T42 horizontal resolution, with 25 vertical levels.
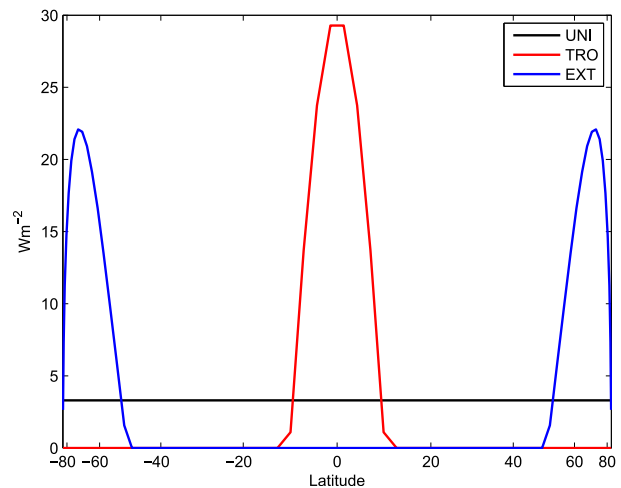

FIG. 1. The zonal-mean prescribed heating H ($\mathrm{W \, m^{-2}}$) for UNI (black), TRO (red), and EXT (blue).

The full GCM, AM2, is run at a horizontal resolution of $2°$ latitude $\times 2.5°$ longitude and 24 vertical levels. To understand the effects of water vapor and cloud–radiative feedbacks and to enable direct comparison with GRaM, the same experiments are performed with fixing the cloud distribution and water vapor content in the radiation calculation, denoted as AM2 + N_{cq}. Additional experiments are performed with the model with prescribed clouds only, denoted as AM2 + N_c. Details on simulations with prescribed clouds and water vapor can be found at Kang et al. (2008, 2009).

To study the dependence of climate response on meridional structure of thermal forcing, the experiments are designed to warm the globe either by weakly heating the whole globe or by strongly heating the narrow tropical or extratropical band, as shown in Fig. 1. In one case, the thermal forcing H is prescribed beneath the mixed layer that provides heating of $3.3 \, \mathrm{W \, m^{-2}}$ uniformly at all latitudes, which is referred to as UNI. In another case, referred to as TRO, H is concentrated over $10°S–10°N$ with the maximum amplitude of $30 \, \mathrm{W \, m^{-2}}$ at the equator. In the third case, referred to as EXT, H is prescribed poleward of $50°$ in both hemispheres with the maximum amplitude of $22 \, \mathrm{W \, m^{-2}}$ at $70°$ in the Northern and Southern Hemispheres. The global mean of H is constrained to be the same in all cases. For reference, the anomalous equatorial surface fluxes during strong El Niño events are confined to $10°S–10°N$ with the maximum amplitude of about $10 \, \mathrm{W \, m^{-2}}$ near the equator, similar to H in TRO. On the other hand, UNI is to mimic the CO_2 forcing. We note that radiative forcing of CO_2 displays some spatial variations, larger in the tropics and subtropics than in the polar region (Fig. 5 in Hansen et al. 2005), but much smoother in latitude than H in TRO. In
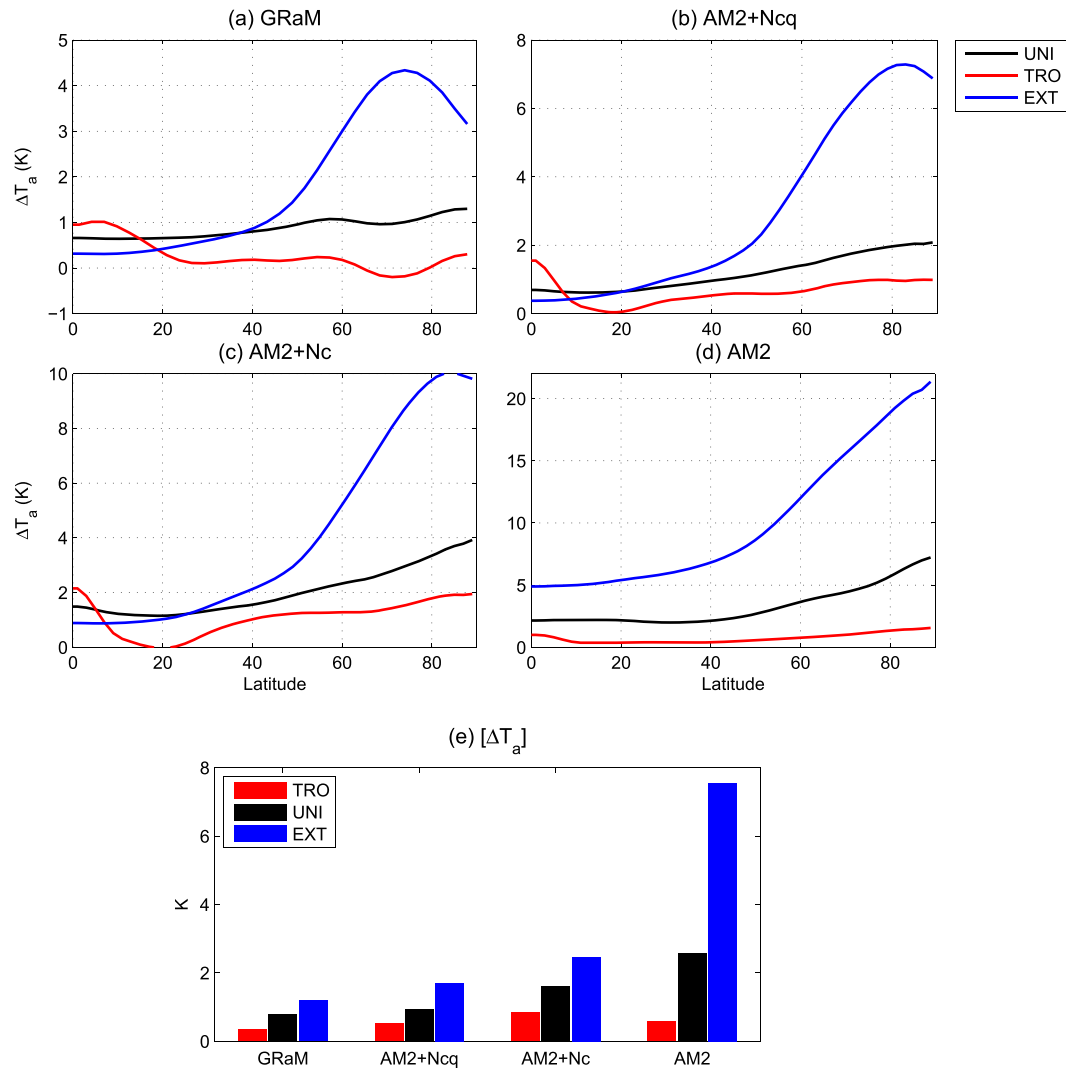
FIG. 2. The zonal-mean temperature response (K) at the lowest model level in (a) GRaM, (b) AM2 with prescribed clouds and water vapor, (c) AM2 with prescribed clouds, and (d) full AM2 for UNI (black), TRO (red), and EXT (blue). (e) The global-mean temperature response at the lowest model level in all experiments.

EXT, H can be thought of as perturbations in the surface energy budget resulting from diminishing polar sea ice cover. The control integration is symmetric about the equator, without imposed surface flux anomalies. The climate response to H is obtained by differencing the climatologies of the perturbed and control integrations, and is denoted as Δ. The time mean fields are calculated by averaging the Northern and Southern Hemispheres since the prescribed surface flux and the resulting model climatology are hemispherically symmetric.

3. Simplified model results

We first discuss the results from GRaM where complications from water vapor and cloud radiative feedbacks

are absent. The zonal-mean response of temperature in the lowest atmospheric level (ΔT_a) is shown in Fig. 2a. We note that the results using sea surface temperature is qualitatively the same. At the equator, the prescribed heating is 10 times larger in TRO than in UNI, but ΔT_a there differs only by 20%. However, in the extratropics, ΔT_a is proportional to the prescribed heating: ΔT_a poleward of 50° in both hemispheres is 3 times larger in EXT than in UNI, with little change in TRO. Also, despite the absence of sea ice albedo feedback and the uniformity of the prescribed heating in UNI, ΔT_a increases with latitude: ΔT_a poleward of 70° in both hemispheres is 70% larger than ΔT_a between 10°S and 10°N. The mechanism of polar amplification has been investigated in previous studies (e.g., Alexeev et al. 2005; Cai 2005; Bintanja et al. 2011).
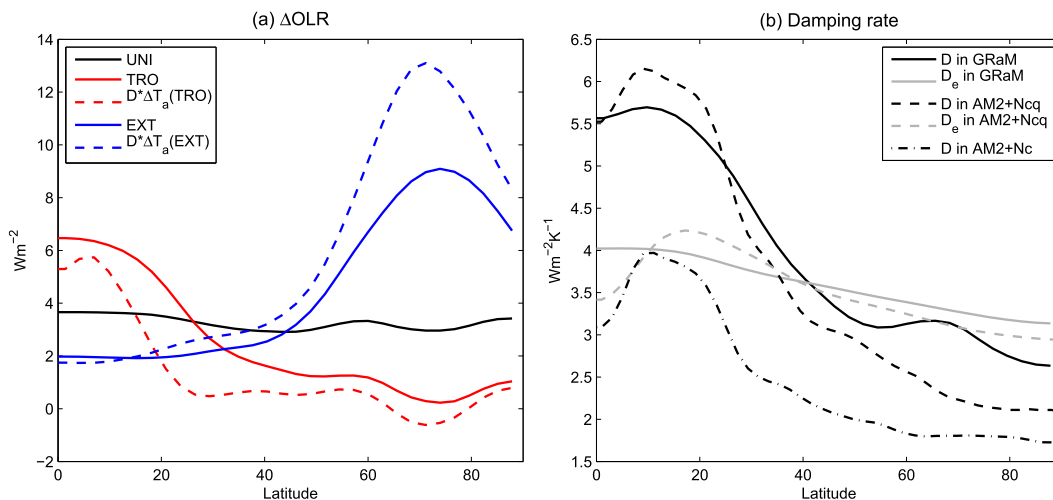
FIG. 3. (a) Zonal-mean changes in OLR (W m^{-2}) for UNI (black), TRO (red), and EXT (blue). (b) The damping rate ($D = \Delta OLR/\Delta T_a$; black) and the effective damping rate ($D_e = \Delta OLR/\Delta T_e$; gray) in GRaM (solid), AM2 with prescribed clouds and water vapor (dashed), and AM2 with prescribed clouds (dash-dotted); unit is W m^{-2} K^{-1}. Dashed line in (a) indicates the prediction of ΔOLR from D in (b).

As a result, although the global mean of prescribed heating is identical in all cases, the global mean of ΔT_a, denoted as $[\Delta T_a]$, is starkly different, as shown in Fig. 2e. This indicates that adding heat to the extratropics, as compared to the tropics, much more efficiently increases the global surface temperature. In other words, the tropics can balance the imposed heating much more effectively with only a small change in surface temperature.

In terms of global mean, the imposed heating beneath the mixed layer has to be balanced by increasing TOA radiative fluxes. In GRaM, the TOA shortwave fluxes are fixed, so that the TOA energy budget is determined by outgoing longwave radiation (OLR). Figure 3a shows the zonal-mean response of OLR. Compared to ΔT_a in Fig. 2a, ΔOLR is smoother in latitude, with almost flat meridional structure in UNI. The sensitivity of ΔOLR to ΔT_a that measures the local radiative damping rate, denoted as $D \equiv \Delta OLR/\Delta T_a$, is shown as black solid in Fig. 3b. The damping rate D is obtained from the UNI profile since ΔT_a in other cases has sharp peaks that cause D to be ill defined. The response of OLR can be predicted from D given the actual ΔT_a, as can be seen from the gross similarity of meridional structure between the actual (solid) and the predicted (dashed) ΔOLR in TRO and EXT in Fig. 3a.

The damping rate D is a function of latitude, with larger values in the tropics. Specifically, D in the tropics (5.6 W m^{-2} K^{-1} over 20°S–20°N) is almost twice as large as that in the polar region (3.0 W m^{-2} K^{-1} over 50°–90° in both hemispheres). This indicates that the tropics can

emit larger amount of OLR for given ΔT_a than the extratropics, so that the heating with an equatorial peak is effectively damped to produce small ΔT_a whereas the heating concentrated in the extratropics is inefficiently damped to produce large ΔT_a. The larger damping in the tropics can be understood from the vertical structure of temperature changes, shown in Fig. 4 (left). Overlain in black solid lines are the effective emission level z_e defined as the level at which the temperature is equal to the effective emission temperature $T_e = (OLR/\sigma)^{1/4}$, where σ is the Stefan–Boltzmann constant.

In the tropics, the temperature closely follows the moist adiabat to result in a maximum warming near the tropopause in all cases. The high z_e in the tropics then leads to large radiative damping there. In contrast, in the extratropics poleward of 60°, TRO produces an elevated warming with a peak at 550 hPa while EXT produces a surface trapped warming, consistent with Alexeev et al. (2005). The stronger polar surface warming is due to the stably stratified atmosphere that tends to trap heat near the surface, which has been invoked as the mechanism for polar amplification (e.g., Bintanja et al. 2011). In UNI, the extratropical temperature response can be characterized as the sum of tropical-induced elevated warming and local-induced surface warming. The elevated warming is subject to strong radiative damping, whereas the surface trapped warming hides beneath z_e and is subject to only weak radiative damping. Hence, a large ΔT_a in the extratropics is required to balance the imposed heating due to surface trapped warming below z_e, leading to inefficient damping rate (i.e., small D).
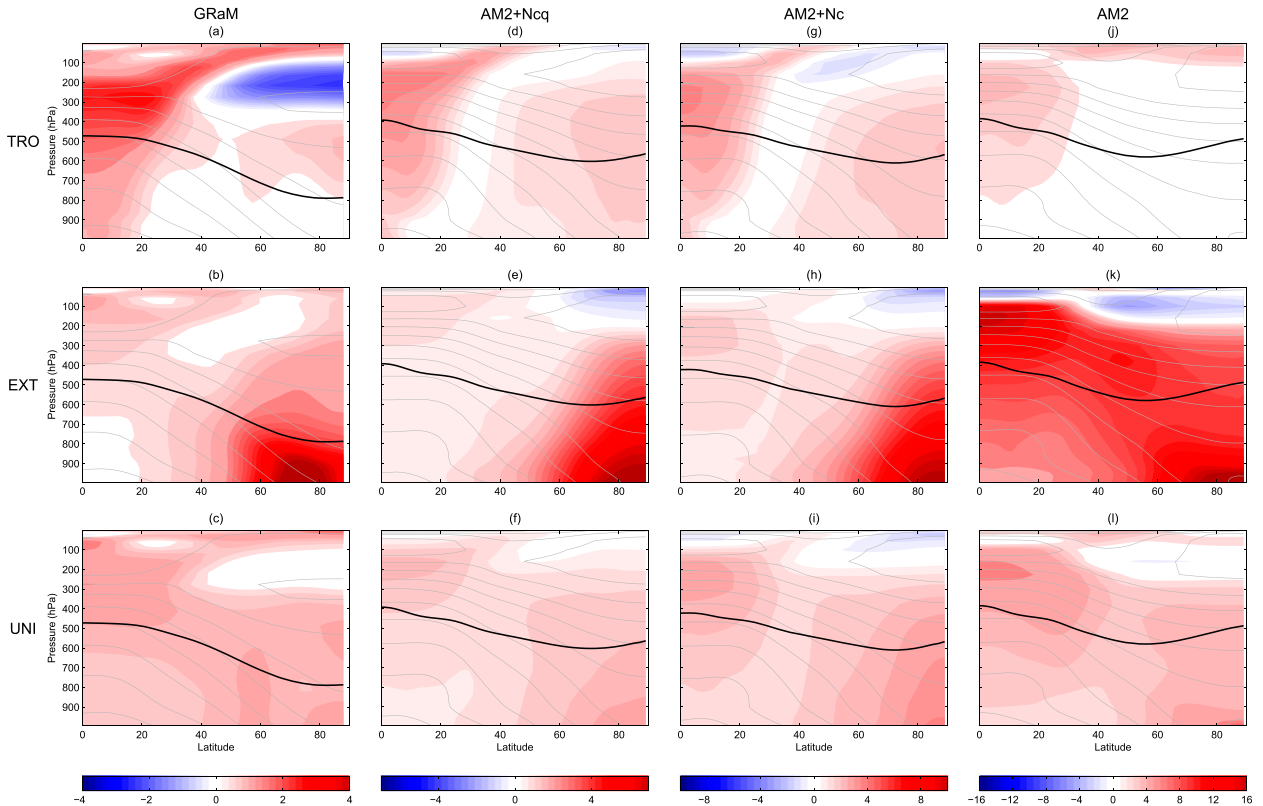
FIG. 4. Zonal-mean changes in temperature (K) for (top) TRO, (middle) EXT, and (bottom) UNI in (a)–(c) GRaM, (d)–(f) AM2 with prescribed clouds and specific humidity, (g)–(i) AM2 with prescribed clouds, and (j)–(l) full AM2. The gray contours indicate the mean temperature in the control integration with a contour interval of 10 K. The black line indicates the effective emission level in the control integration.

Conversely, in the tropics, the imposed heating can be balanced by small ΔT_a due to the amplification of warming aloft above z_e, which results in effective damping rate (i.e., large D). Therefore, although the global mean of imposed heating is constrained to be the same, the heating with an equatorial peak (TRO) produces much smaller increase in $[\Delta T_a]$ than the heating confined to the extratropics (EXT).

The more effective OLR damping in the tropics can occur partly because OLR is a strong function of temperature (i.e., OLR = σT_e^4), as suggested by Joshi et al. (2003). The importance of its effect can be estimated by defining the damping rate in terms of ΔT_e (i.e., $D_e \equiv \Delta OLR/\Delta T_e = 4\sigma T_e^3$), shown as gray solid in Fig. 3b. The value of D_e in the tropics (4.0 W m^{-2} K^{-1} over 20°S–20°N) is 17% larger than that in the polar region (3.3 W m^{-2} K^{-1} over 50°–90° in both hemispheres), much smaller than the latitudinal contrast of D that amounts to 100%. Thus, the contrast of vertical structure of warming between the tropics and polar region is more important in causing a larger OLR damping in the tropics, hence a smaller $[\Delta T_a]$ in TRO.

4. Comprehensive model results

The effect of water vapor– and cloud–radiative feedbacks on the global surface warming can be addressed by comparing the results between GRaM and AM2. In AM2, over the intertropical convergence zone (ITCZ), shortwave cloud forcing associated with low cloud amount changes tends to be larger than longwave cloud forcing associated with high cloud amount changes, as noted in Kang et al. (2008). As shown in Fig. 5, low cloud amount increase in TRO results in cooling by 18 W m^{-2} in the equatorial region. The negative cloud feedback in the tropics is absent in UNI and reverses sign in EXT. This suggests that the tropical cloud feedback is a response not to local temperature changes but rather to large-scale changes in circulation. The Hadley circulation is strengthened in TRO to increase cloudiness, inducing the negative cloud feedback. In contrast, the heating in UNI has little effect on the Hadley circulation and the heating in EXT weakens it. In the extratropics, low cloud amount decreases substantially in EXT because the atmosphere is destabilized as the temperature and
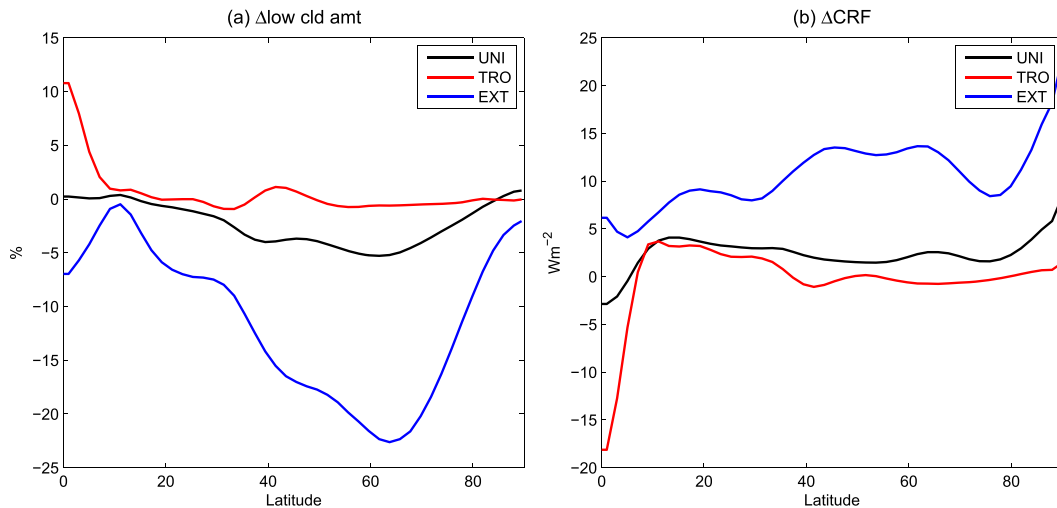
FIG. 5. Zonal-mean changes in (a) low cloud amount (%) and (b) total cloud radiative forcing (W m^{-2}) for UNI (black), TRO (red), and EXT (blue) in full AM2.

humidity near the surface increase, resulting in increased surface insolation of up to 15 W m^{-2}. Such a large change in cloud distribution could be due to the fact that heating is prescribed at the surface, producing extreme destabilizing effects on the atmosphere. Hence, the effect of clouds may be reduced for tropospheric heating. In AM2, the cloud forcing acts to amplify the extratropical thermal forcing, whereas it acts to damp the tropical thermal forcing. Hence, one can expect that the dependence of $[\Delta T_a]$ on the latitudinal position of thermal forcing will be more enhanced in AM2 than in GRaM.

The zonal-mean temperature response at the lowest model level, ΔT_a for AM2 is shown in Fig. 2d. In TRO, the negative cloud forcing over the ITCZ damps the equatorial peak of ΔT_a so effectively that the tropical ΔT_a is even smaller than in GRaM despite the positive water vapor feedback that greatly amplifies the response. Also, because of the negative feedback from clouds in the tropics, ΔT_a in the tropics is the smallest when heating is prescribed within the tropics and is the largest when heating is prescribed in the polar region. This is because in EXT, the tropical temperature response is not accompanied by negative cloud forcing in the tropics (Fig. 4j–l). In EXT, the positive cloud forcing in the extratropics as well as the positive water vapor feedback amplify ΔT_a, resulting in 6 times larger response than that in GRaM. As a result, there is greater dependence of global-mean ΔT_a on the meridional structure of thermal forcing in AM2 than in GRaM (Fig. 2e). This indicates that cloud radiative feedbacks can alter the efficiency of climate forcing for warming the surface, implying that the degree of contrast will be model dependent. In AM2, the same global-mean surface heating, depending on its

meridional position, can produce global warming of different magnitude by a factor of 13. It came to our attention that Rose et al. (2014) performed similar experiments and showed that extratropical forcing is more effective at changing the global mean surface temperature. However, the difference in response is much smaller, only a factor of 3, between the extratropical and tropical forcing. The discrepancy would be due to differences in the experiment design. Our heating is applied equatorward of 10° in the tropical case and poleward of 50° in the extratropical case, whereas cooling is applied in broader regions in Rose et al. (2014), equatorward of 30° in the tropical case and poleward of 40° in the extratropical case. Therefore, the difference in lapse rate and cloud feedbacks between the tropical and extratropical forcing cases is more pronounced in our study. More fundamentally, the subtropical cloud response in the tropical forcing case and the midlatitude cloud response in the extratropical forcing case are shown to offset the cloud response in the deep tropics and in high latitudes, respectively (Figs. 2b and 2c in Rose et al. 2014), which do not occur in our experiments since no heating is applied there. There could also be some nonlinear effects to enhance the response to warming relative to the response to cooling.

To better compare with GRaM and to examine the robustness of the results, experiments are performed with fixed clouds only (AM2 + N$_c$) or fixed clouds and water vapor content (AM2 + N$_{cq}$) in AM2. In a prescribed cloud model (Figs. 2b and 2c), without negative cloud feedback in the tropics, the tropical ΔT_a becomes largest in TRO, as in GRaM (Fig. 2a). The AM2 + N$_{cq}$ experiment displays a similar response to GRaM, which

has no clouds or water vapor feedbacks: both models exhibit larger ΔT_a in EXT than in TRO by a factor of 3.3. As shown in Fig. 3b, the damping rate also exhibits a similar latitudinal profile between the two models, indicating that similar mechanisms are at effect in AM2 as in GRaM. The vertical profile of temperature response shown in Fig. 4 is also similar, exhibiting a maximum warming near the tropopause in the tropics and at around 500 hPa at the pole in TRO and surface trapped warming in the extratropics in EXT. The vertical structure of warming causes the OLR damping to be more effective in the tropics, leading to a smaller ΔT_a when heating is located in the tropics than in the extratropics.

The effect of water vapor feedback can be diagnosed by a comparison between AM2 + N_{cq} and AM2 + N_c. The overall response is amplified by water vapor feedback (Figs. 2b and 2c), which is consistent with reduced radiative damping rate (Fig. 3b). The response is amplified by a larger amount in EXT than in TRO (Fig. 2e): $[\Delta T_a]$ in AM2 + N_c is larger than that in AM2 + N_{cq} by 60% in TRO as opposed to 70% in EXT. The tropics with a larger increase in water vapor content (more positive water vapor feedback) also exhibit a larger tropospheric warming (stronger radiative damping) (e.g., Soden and Held 2006). The former (latter) tends to amplify (weaken) $[\Delta T_a]$ more in TRO, as compared with EXT. Here, larger negative lapse rate feedback in the tropics overcompensates positive water vapor feedback, resulting in a smaller $[\Delta T_a]$ increase in TRO than in EXT.

5. Discussion

We show that the magnitude of global warming, which is measured as the global-mean response of temperature at the lowest model level, depends on the meridional structure of surface thermal forcing. The experiments are performed with an idealized GCM, in which water vapor– and cloud–radiative feedbacks are excluded, and a full GCM, both of which are coupled to an aquaplanet slab mixed layer ocean. The heating, often called Q flux, is prescribed in different latitudinal bands beneath the mixed layer. Both models produce the largest (least) global-mean surface warming when the surface heating is confined to a narrow polar (tropical) region. In the idealized GCM, the difference is a factor of 3.3, and this difference is amplified in the full GCM to a factor of 13. The enhanced contrast between the TRO and EXT runs in the full GCM is mostly due to clouds that act as a negative feedback in the tropics and a positive feedback in the extratropics. The full GCM with prescribed clouds and water vapor exhibits a similar response to the idealized model, confirming the robustness of the results when radiative feedbacks are inhibited.

When globally averaged, the imposed heating is balanced by net TOA radiation. A larger fraction of the heating is radiated directly to space when the temperature response is maximized aloft (above the effective radiation level), leading to weak warming near the surface. In contrast, the surface trapped temperature response cannot effectively emit OLR, requiring strong warming near the surface. Therefore, the heating confined to the tropics, where the maximum warming occurs near the tropopause following a moist adiabat, is effectively damped to result in weak global surface warming. In the extratropics, the temperature response to local heating is trapped near the surface, requiring large surface warming to emit enough OLR. This indicates that the damping rate of imposed heating is large in the tropics and small in the extratropics, suggesting that the tropical heating will be balanced by smaller surface warming than the extratropical heating. This latitudinal dependence of radiative damping rate is the fundamental reason for the stark dependence of magnitude of global surface warming on the meridional structure of thermal forcing.

These results suggest that the efficiency of localized climate forcing agent such as aerosols for warming the global surface may strongly depend on its latitudinal position, with polar sources being more effective than tropical sources. However, we note that the results herein may be at an extreme limit because of the way we designed the experiments. First, the aquaplanet mixed layer setting produces a strong Hadley circulation that leads to a sharp ITCZ with almost completely dry subtropics (Frierson et al. 2006). The clouds associated with the ITCZ are concentrated in the narrow region, which may be partly responsible for a large negative cloud forcing in the tropics that effectively damps tropical surface warming. Second, if the heating is prescribed in the troposphere rather than at the surface, the impact on the tropical lapse rate will be smaller and the temperature response at the pole will be less bottom-heavy. Also, the tropospheric warming may have a less destabilizing effect in the extratropics, which may reduce the strength of positive cloud feedback. Still, larger global surface warming is expected to extratropical heating than to tropical heating regardless of the level of the prescribed heating, as shown by Hansen et al. (1997).

Ocean upwelling in the equatorial Pacific displays strong interannual-to-multidecadal variability. Our tropical forcing case is to mimic such El Niño–like heating due to natural variability of equatorial upwelling. The equatorial ocean forcing is shown to be important for modulating the decadal trend of global temperature (Kosaka and Xie 2013). This is perplexing in light of our result that the equatorial forcing is ineffective in inducing global

mean temperature response. Thus, the equatorial Pacific variability is important for global mean temperature not because of the former's efficiency for the latter, but rather because the mean upwelling makes it a preferred mode of natural variability.

REFERENCES

Alexeev, V. A., P. L. Langen, and J. R. Bates, 2005: Polar amplification of surface warming on an aquaplanet in "ghost forcing" experiments without sea ice feedbacks. *Climate Dyn.,* **24,** 655–666, doi:10.1007/s00382-005-0018-3.

Anderson, J. L., and Coauthors, 2004: The new GFDL global atmosphere and land model AM2–LM2: Evaluation with prescribed SST simulations. *J. Climate,* **17,** 4641–4673, doi:10.1175/JCLI-3223.1.

Bintanja, R., R. G. Graversen, and W. Hazeleger, 2011: Arctic winter warming amplified by the thermal inversion and consequent low infrared cooling to space. *Nat. Geosci.,* **4,** 758–761, doi:10.1038/ngeo1285.

Cai, M., 2005: Dynamical amplification of polar warming. *Geophys. Res. Lett.,* **32,** L22710, doi:10.1029/2005GL024481.

Forster, P. M., M. Blackburn, R. Glover, and K. P. Shine, 2000: An examination of climate sensitivity for idealised climate change experiments in an intermediate general circulation model. *Climate Dyn.,* **16,** 833–849, doi:10.1007/s003820000083.

Frierson, D. M. W., 2007: The dynamics of idealized convection schemes and their effect on the zonally averaged tropical circulation. *J. Atmos. Sci.,* **64,** 1959–1976, doi:10.1175/JAS3935.1.

——, I. M. Held, and P. Zurita-Gotor, 2006: A gray-radiation aquaplanet moist GCM. Part I: Static stability and eddy scale. *J. Atmos. Sci.,* **63,** 2548–2566, doi:10.1175/JAS3753.1.

Hansen, J., M. Sato, and R. Ruedy, 1997: Radiative forcing and climate response. *J. Geophys. Res.,* **102,** 6831–6864, doi:10.1029/96JD03436.

——, and Coauthors, 2005: Efficacy of climate forcings. *J. Geophys. Res.,* **110,** D18104, doi:10.1029/2005JD005776.

Joshi, M., K. Shine, M. Ponater, N. Stuber, R. Sausen, and L. Li, 2003: A comparison of climate response to different radiative forcings in three general circulation models: Towards an improved metric of climate change. *Climate Dyn.,* **20,** 843–854, doi:10.1007/s00382-003-0305-9.

Kang, S. M., I. M. Held, D. M. W. Frierson, and M. Zhao, 2008: The response of the ITCZ to extratropical thermal forcing: Idealized slab-ocean experiments with a GCM. *J. Climate,* **21,** 3521–3532, doi:10.1175/2007JCLI2146.1.

——, D. M. W. Frierson, and I. M. Held, 2009: The tropical response to extratropical thermal forcing in an idealized GCM: The importance of radiative feedbacks and convective parameterization. *J. Atmos. Sci.,* **66,** 2812–2827, doi:10.1175/2009JAS2924.1.

Knutti, R., and G. C. Hegerl, 2008: The equilibrium sensitivity of the Earth's temperature to radiation changes. *Nat. Geosci.,* **1,** 735–743, doi:10.1038/ngeo337.

Kosaka, Y., and S.-P. Xie, 2013: Recent global-warming hiatus tied to equatorial Pacific surface cooling. *Nature,* **501,** 403–408, doi:10.1038/nature12534.

Ramaswamy, V., and Coauthors, 2001: Radiative forcing of climate change. *Climate Change 2001: The Scientific Basis,* J. T. Houghton et al., Eds., Cambridge University Press, 349–416.

Rose, B. E. J., K. C. Armour, D. S. Battisti, N. Feldl, and D. D. B. Koll, 2014: The dependence of transient climate sensitivity and radiative feedbacks on the spatial pattern of ocean heat uptake. *Geophys. Res. Lett.,* **41,** 1071–1078, doi:10.1002/2013GL058955.

Soden, B. J., and I. M. Held, 2006: An assessment of climate feedbacks in coupled ocean–atmosphere models. *J. Climate,* **19,** 3354–3360, doi:10.1175/JCLI3799.1.

Xie, S.-P., B. Lu, and B. Xiang, 2013: Similar spatial patterns of climate responses to aerosol and greenhouse gas changes. *Nat. Geosci.,* **6,** 828–832, doi:10.1038/ngeo1931.